IEEE Photonics Journal
An IEEE Photonics Society Publication

Open Access

Demonstration of a Silicon Photonic Circuit for Half-Add Operations Using Cascaded Microring Resonators

Volume 9, Number 1, February 2017

Xiaosuo Wu
Lin Deng
Yinghao Meng
Jianhong Yang
Yonghui Tian, ***Member, IEEE***

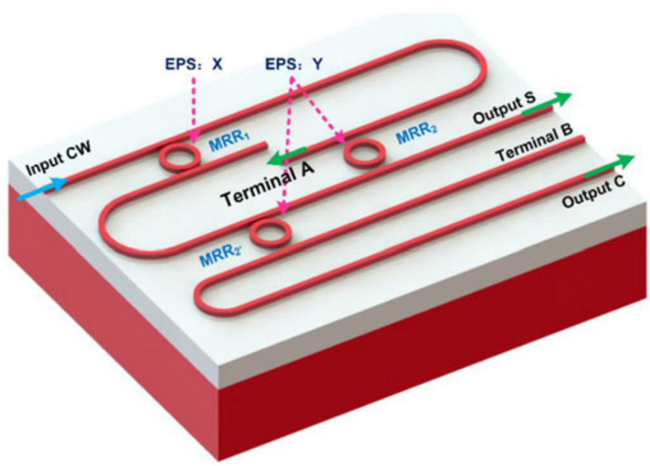

DOI: 10.1109/JPHOT.2016.2639787
1943-0655 © 2016 IEEE

IEEE photonics SOCIETY

IEEE

Demonstration of a Silicon Photonic Circuit for Half-Add Operations Using Cascaded Microring Resonators

Xiaosuo Wu, Lin Deng, Yinghao Meng, Jianhong Yang, and Yonghui Tian, *Member, IEEE*

Institute of Microelectronics and Key Laboratory for Magnetism and Magnetic Materials of MOE, School of Physical Science and Technology, Lanzhou University, Lanzhou 730000, Gansu, China

DOI:10.1109/JPHOT.2016.2639787

Manuscript received November 30, 2016; revised December 9, 2016; accepted December 12, 2016. Date of publication December 15, 2016; date of current version February 6, 2017. This work was supported in part by the National Natural Science Foundation of China under Grant 61405082 and in part by the Fundamental Research Funds for the Central Universities. Corresponding author: Y. H. Tian (e-mail: siphoton@lzu.edu.cn).

Abstract: We report a silicon photonic circuit that can perform half-add operations using cascaded microring resonators (MRRs). Electrical pulse sequences regarded as the operands are applied to the corresponding MRRs to achieve their dynamic modulations. The final operation results are directed to the corresponding outputs in the form of light. For proof of principle, the thermo-optic modulation scheme that needs simpler fabrication processes is employed to modulate MRRs. Finally, the circuit is fabricated on an 8-in silicon-on-insulator (SOI) substrate using complementary metal-oxide-semiconductor (CMOS) technology, and the half-add operations with the speed of 10 Kb/s are demonstrated successfully.

Index Terms: Integrated optics, optical resonators, silicon photonics, thermo-optical devices.

1. Introduction

Silicon photonics is a popular research topic in the field of integrated optics whose purpose is to integrate various photonic devices on a tiny silicon wafer to achieve complex optical information processing using standard complementary-metal-oxide-semiconductor (CMOS) fabrication processing [1]–[3]. Currently, silicon photonics has been greatly developed, and diversified photonic devices have been proposed and demonstrated such as routers [4], lasers [5], modulators [6]–[8], logic devices [9]–[11], sensors [12], [13], multiplexers [14], microprocessors [15], etc, and silicon photonic devices are also very suitable for information processing due to its nature advantages such as high speed [16], [17], large capacity [18], [19], low power [20], [21], etc. Therefore, silicon photonics is a promising solution to the problems of limited bandwidth [22], [23], physical limited effect (quantum tunneling) and metal interconnect issue faced by silicon electronics [24], [25]. The microring resonator (MRR) is a fundamental building block for photonic devices [26], and it can be used to structure various photonic devices to achieve different optical information processing functions such as optical filtering [27], modulation [28], [29], switching [30], [31], etc. One of the most important applications of MRR is that it can be designed to high compactness [32], low power

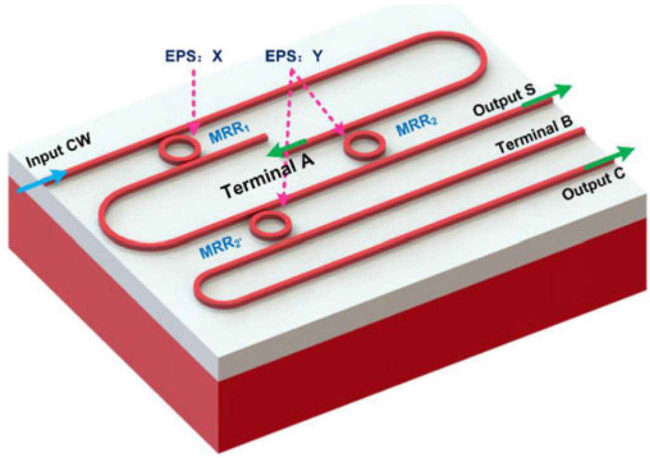

Fig. 1. Architecture of the proposed circuit. (CW: continuous-wave light. EPS: electrical pulse sequence. MRR: micro-ring resonator.)

[33], and high speed optical switch [34], and the optical switch based on MRR is easily to realize on-chip large-scale integration and low fabrication cost [26], [35].

Directed logic proposed by Shamir and Hardy in 2007 is a novel logic scheme which employs optical switch network to perform Boolean logic operations [36], [37]. A continues monochromatic optical wave is coupled into the optical switch network, the operands are applied to the optical switch to control their working status [38], [39]. Therefore, the operand applied to the optical switches in the network can control the propagation direction of the light. In other word, the light signal directed to the output port of the network carries the information of the operand applied to the optical switch. Therefore, we can reasonably design the optical switch network to perform specific logic operation according to our specific requirements [40], and the final operation results are directed to the output port of the network in the form of light [41]. The optical half-adder plays a key role in the optical information processing and optical computing since the half-adder can be employed to structure full-adder through cascading some half-adders [42], [43]. As we know, all logic operations can be attributed to addition and multiplication operations. In other words, if we can achieve addition and multiplication operations, all other complex logic operations can be achieved. Therefore, the optical adder is an important building block for optical information system.

In this paper, we report a novel silicon photonic circuit which can performs half-addition using three cascaded MRRs. The Sum and Carry operation results of the addition could be obtained at its two output ports simultaneously. Compared with our previous works [44], the photonic circuit is simpler, and the multimode interference coupler (MMI) is eliminated in the circuit, which is very significant to improve the signal quality and reduce the insertion loss of the device. As a proof of principle, the thermo-optic modulation scheme is employed to achieve MRR's dynamic modulation, and the circuit is finally fabricated on silicon-on-Insulator (SOI) substrate using the CMOS technology. Finally, the half-add operation is demonstrated with the operation speed of 10 Kbps successfully.

2. Architecture and Working Principle

The schematic of the half-add circuit is shown in Fig. 1. The proposed circuit consisting of only three cascaded MRRs connected by waveguides. Three ports of the circuit are defined as *CW*, *S*, and *C* on the basis of their functions. The port CW behaves as the input port of the half-adder. The ports *S* and *C* serve as the output of the sum bit and the carry bit of the circuit respectively. In the proposed circuit, MRR behaves as the 1×2 optical switch: When a high-level voltage is applied to MRR, it is on-resonance at the working wavelength of λw and the optical signal coupled into its input port is downloaded by the MRR subsequently directs to its drop port. When a low-level voltage is applied

TABLE 1
TRUTH TABLE ACHIEVED BY THE PROPOSED CIRCUIT

EPS		Port S		Port C	
X	Y	Optical Power Level	Logic Value	Optical Power Level	Logic Value
0	0	0 (P)	0	0 (P)	0
0	1	1 (P)	1	0 (P)	0
1	0	1 (P)	1	0 (P)	0
1	1	0 (P)	0	0 (P)	1

to MRR, it is off-resonance at the working wavelength of λw, and the optical signal coupled into its input port bypasses the MRR, thereafter directing to its through port. MRR_1's working state is controlled by the working states of electrical pulse sequence (EPS) X, while MRR_2 and $MRR_{2'}$ are working as a synchronous part since they are modulated by the working states of EPS Y.

In the circuit, the high-level and low-level of the EPS applied to MRR represent logic 1 and 0 in electrical domain, and the high-level and low-level of the optical power at the output port are defined as logic 1 and 0 in optical domain. Monochromatic continuous-wave light with the working wavelength λ_w is coupled into the circuit through the CW port and then modulated by EPSs applied to MRRs. Finally, the operation results appear at the output ports of the circuit in the form of optical pulse. In order to clarify the principle of the circuit, the four working statuses are discussed in more detail as follows.

1) When $X = Y = 0$ (the voltage X applied to MRR_1 and the voltage Y applied to MRR_2 and $MRR_{2'}$ are both at low-level), all of the MRRs are at off-resonance at the working wavelength of λ_w. The light signal coupled into the *CW* port of the circuit first bypasses MRR_1. Then, the optical signal bypasses MRR_2 and is finally directed to the terminal *A*. As a result, logical 0 is achieved at the output ports *S* and *C* with the working wavelength of λ_w ($S = 0$, $C = 0$).
2) When $X = 0$ and $Y = 1$ (the voltage X applied to MRR_1 is at the low-level and the voltage Y applied to MRR_2 and $MRR_{2'}$ is at high level, respectively), the MRR_1 is at off-resonance. MRR_2 and $MRR_{2'}$ are both at on-resonance, since MRR_2 and $MRR_{2'}$ are working as a synchronous part. The light signal coupled into the *CW* port of the circuit firstly bypasses MRR_1 and is then downloaded by MRR_2, eventually directing to the *S* port, which means that logical 1 is achieved at the output port *S*, and logical 0 is achieved at the output port *C* with the working wavelength of λ_w ($S = 1$, $C = 0$).
3) When $X = 1$ and $Y = 0$ (the voltage X applied to MRR_1 is at high-level while the voltage Y applied to MRR_2 and $MRR_{2'}$ is at low level, respectively), MRR_1 is at on-resonance, while MRR_2 and $MRR_{2'}$ are both at off-resonance. The light signal coupled into the *CW* port of the circuit firstly downloaded by MRR_1 and then bypasses MRR_2 and $MRR_{2'}$ successively and ultimately directed to the *S* port. Consequently, logical 1 is achieved at the output port *S* and logical 0 is achieved at the output port *C* with the working wavelength of λ_w ($S = 1$, $C = 0$).
4) When $X = 1$ and $Y = 1$(the voltages applied to MRR_1, MRR_2 and $MRR_{2'}$ are at high level), all the MRRs are at on-resonance with the working wavelength of λ_w, the light signal coupled into the CW port of the circuit downloaded by MRR_1 and $MRR_{2'}$ successively, then directed to the port *C*. Therefore, logical 1 is achieved at the output port *C*, and logical 0 is achieved at the output port *S* with the working wavelength of λ_w ($S = 0$, $C = 1$).

In order to illuminate the principle of the proposed circuit clearly, the theoretical optical power levels at the output ports of the circuit with four working statuses are shown in the Table I, and

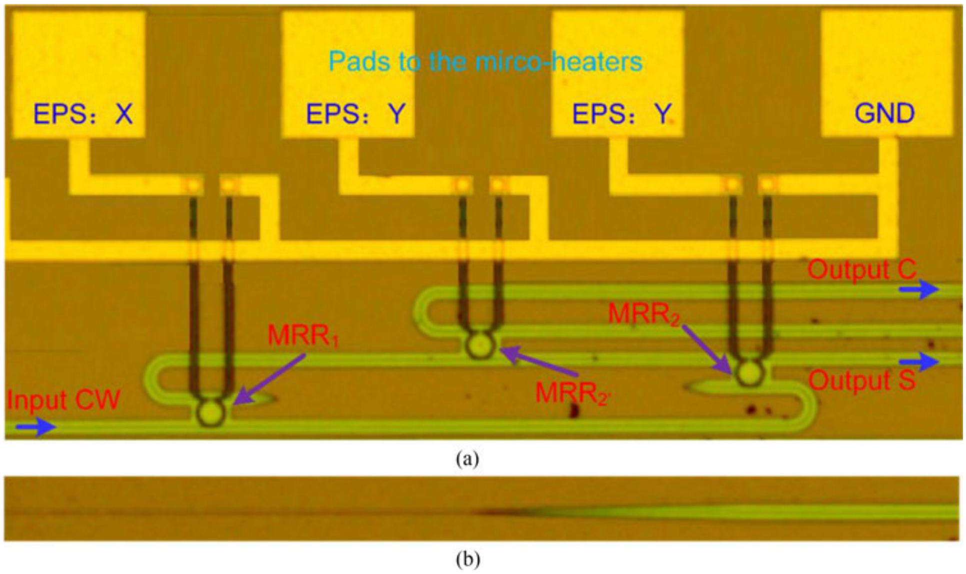

Fig. 2. (a) Micrograph of the circuit. (CW: continuous wave. EPS: electrical pulse sequence. MRR: micro-ring resonator.) (b) Spot size converters.

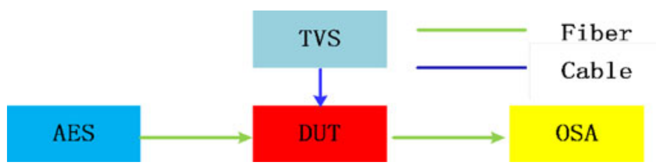

Fig. 3. Experiment schematic for the device's static response. AES: amplified broadband emission source. TVS: tunable voltage source. DUT: device under test. OSA: optical spectral analyzer.

from which we can see clearly that the circuit can perform the adding function of two binary numbers [45].

3. Design and Fabrication

The half-adder circuit is fabricated on an 8-inch SOI wafer with 220 nm top silicon layer and 2 μm buried SiO_2 layer using the CMOS technology. The micrograph of the circuit is shown in Fig. 2(a). In order to reduce the scattering loss induced by the sidewalls of the waveguides and maintain single mode propagation, the rib waveguide with a slab thickness of 90 nm, width of 400 nm and height of 220 nm is employed to form the circuit. The radius of the MRRs are 10 μm, and the gap between the ring waveguide and straight is 350 nm. The titanium nitride (TiN) micro-heaters are fabricated on top of the MRRs. Aluminum wires are formed to connect the pads and the micro-heaters. Furthermore, with a view to enhance the coupling efficiency, spot size converters (see Fig. 2(b)) are designed on the terminals of the circuit [46].

4. Experimental Results and Discussion

Experimental tests of the circuit could be divided into static and dynamic response tests.

4.1. Static Response Test

In order to determine the working wavelength and the working voltages of the circuit, the static response spectra of the circuit should be measured first. As shown in Fig. 3, an optical spectrum

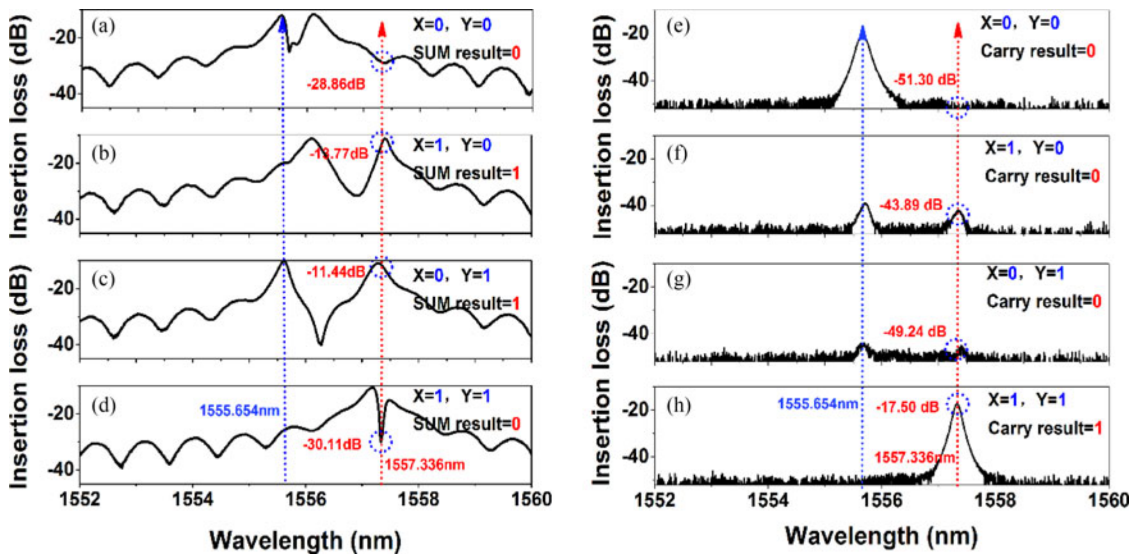

Fig. 4. Response spectra of the circuit at the Output port S (a)–(d) and C (e)–(h) with the applied voltages to MRR_1, $MRR_{2'}$ and MRR_2 being 0 V, 0 V, and 0 V [(a)–(e)], 2.91 V, 0 V, and 0 V. (b)–(f) 0 V, 2.12 V and 2.05 V [(c),(g)], 2.91 V, 2.12 V, and 2.05 V [(d)–(h)].

analyzer (OSA), three tunable voltage sources (TVSs), and an amplified broadband spontaneous emission source (AES) are employed in the experiment scheme. A lensed fiber is used to couple the broadband wave light into the *CW* port of the circuit. And the output light of the circuit is directed into the OSA through another lensed fiber. Although the physical parameters of the circuit are designed to be identical, two tunable voltage sources should be applied to compensate the slight deviation caused by the limitation of fabrication accuracy. A redshift can be measured when the MRR is heated up by the tunable voltage source, arising from the effective refractive index of the ring increases [47]. Bias voltage of 0.86 V and 0.08 V are applied to the micro-heaters above MRR_1 and $MRR_{2'}$ respectively, in order to make MRRs have the same resonant wavelength of 1555.654 nm which is regarded as the initial state of the circuit. In principle, wavelength longer than 1555.654 nm could be chosen as the working wavelength. Wavelength of 1557.336 nm is chosen as the working wavelength as to achieve a large extinction ratio with low power consumption. The static response spectra of the circuit at the output port *S* are shown in Fig. 4(a)–(d), and the static response spectra at the output port *C* are shown in Fig. 4(e)–(h).

The static response spectra at the port *S* with no voltages applied to the MRRs is shown in Fig. 4(a). When the voltage applied to MRR_1 increases to 2.91 V, MRR_1's resonance wavelength is shifted to the working wavelength λ_w, and the others still resonate at the initial state. Therefore, the static response spectra at the port *S* shows the drop filtering characteristics of MRR_1 and the through filtering characteristics of $MRR_{2'}$ and MRR_2. And the response spectra at the output port *S* is shown in Fig. 4(b). When the voltages applied to $MRR_{2'}$ and MRR_2 are 2.12 V and 2.05 V, respectively, those two MRR's resonance wavelength will be shifted to the working wavelength λ_w, while MRR_1 still resonate at the initial state. Hence the response spectra at the port *S* shows the through filtering characteristics of MRR_1 and the drop filtering characteristics of MRR_2, as shown in Fig. 4(c). When the voltages applied to MRR_1, $MRR_{2'}$ and MRR_2 are 2.91 V, 2.12 V and 2.05 V, respectively, their resonance wavelengths are shifted to the working wavelength λ_w. The result is that there is a dip located at 1557.336 nm and the static response spectra at the port *S* is shown in Fig. 4(d).

It is obviously that the insertion loss at the working wavelength λ_w is about −28.86 dB when $X = 0$ and $Y = 0$ (see Fig. 4(a)), while the insertion loss at the working wavelength λ_w is about −30.11 dB when $X = 1$ and $Y = 1$ (see Fig. 4(d)). Although the insertion levels are different at these two working statuses, both of them could be considered as the low level and the optical power at the

TABLE 2
EXPERIMENTAL INSERTION LOSS, OPTICAL POWER LEVELS AND LOGICAL VALUE WITH WORKING WAVELENGTH AT THE OUT PORTS OF THE CIRCUIT

EPS		Port S			Port C		
X	Y	Insertion Loss	Power level	Logical Value	Insertion Loss	Power level	Logical Value
0	0	-28.86 (dB)	low	0	-51.30 (dB)	low	0
0	1	-13.77 (dB)	high	1	-43.89 (dB)	low	0
1	0	-11.44 (dB)	high	1	-49.24 (dB)	low	0
1	1	-30.11 (dB)	low	0	-17.50 (dB)	high	1

port S is low (logical 0). On the other hand, the insertion loss at the working wavelength λ_w is about -13.77 dB when $X = 1$ and $Y = 0$ (see Fig. 4(b)), while the insertion loss at the working wavelength λ_w is about -11.44 dB when $X = 0$ and $Y = 1$ (see Fig. 4(c)). Both of them could be considered as the high level and the optical power at the port S is high (logical 1). The insertion losses get a slight deviation due to their different routing paths. Analogous to the concept of logic swing level in the electrical domain, the difference of insertion losses with the working wavelength λ_w between the high-level and low-level at the port S is equal to 15.09 dB.

The static response spectra at the port C show the drop filtering characteristics of MRR_1 and $MRR_{2'}$. Only when the voltages applied to MRR_1 and $MRR_{2'}$ are 2.91 V and 2.12 V, respectively, a peak appears at the working wavelength λ_w. The insertion loss with the working wavelength λ_w is about -17.50 dB, and the optical power at the port C is high (logical 1), as shown in Fig. 4(h). In other working statuses, the insertion losses at the working wavelength λ_w are -51.30 dB (see Fig. 4(e)), -43.89 dB (see Fig. 4(f)), and -49.24 dB (see Fig. 4(g)), respectively. Although the optical power levels are different, all of them could be considered as the low level and the optical power at the port C is low (logical 0). The difference insertion losses with the working wavelength λ_w between the high-level and low-level at the port C is equal to 26.39 dB.

All eight static response spectra for the half-add circuit have been analyzed for logical combinations. Note that the bandwidth of the ring is about 0.16 nm, and the Q (quality factor) of the ring resonator is about 9733. Table II shows the measured insertion loss of the circuit at the output ports S and C with four working statuses, which is consistent with the theoretical values shown in Table I. Clearly, the static response spectra of the circuit indicate that the circuit can implement the half-add operations with high noise immunity due to their large logic swing.

4.2. Dynamic Response Test

In the following, the dynamic response of the circuit is characterized by experiment. The experiment schematic for the device's dynamic response is shown in Fig. 5. A tunable laser (TL), two tunable voltage source (TVSs), two arbitrary function generators (AFGs), a two-channel oscilloscope (OSC), an erbium doped fiber amplifier (EDFA), and an optical filter and a photo-detector (PD) are employed to characterize the device's dynamic response.

Firstly, a proper voltage supplied by the tunable voltage source is employed to MRR_1 and $MRR_{2'}$ to eliminate the fabrication errors, in order to guarantee the same resonant wavelength of MRRs at the original state [48], [49]. Monochromatic continuous-wave light generated by a C-band tunable laser with the wavelength λ_w of 1557.336 nm first directs into a polarization controller, and then, the light with TE polarization is coupled into the CW port of the circuit. The output optical signals at

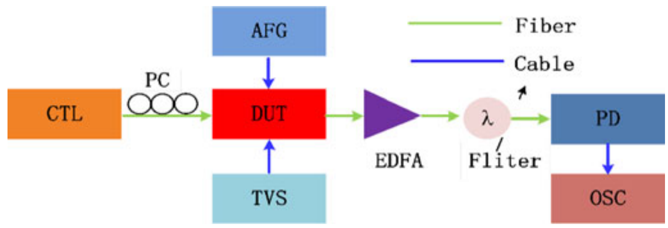

Fig. 5. Experiment schematic for the circuit's dynamic response. CTL: C-band tunable laser. PC: polarization controller. DUT: device under test. TVS: tunable voltage source. AFG: arbitrary function generator. EDFA: erbium doped fiber amplifier. PD: photo-detector. OSC: oscilloscope.

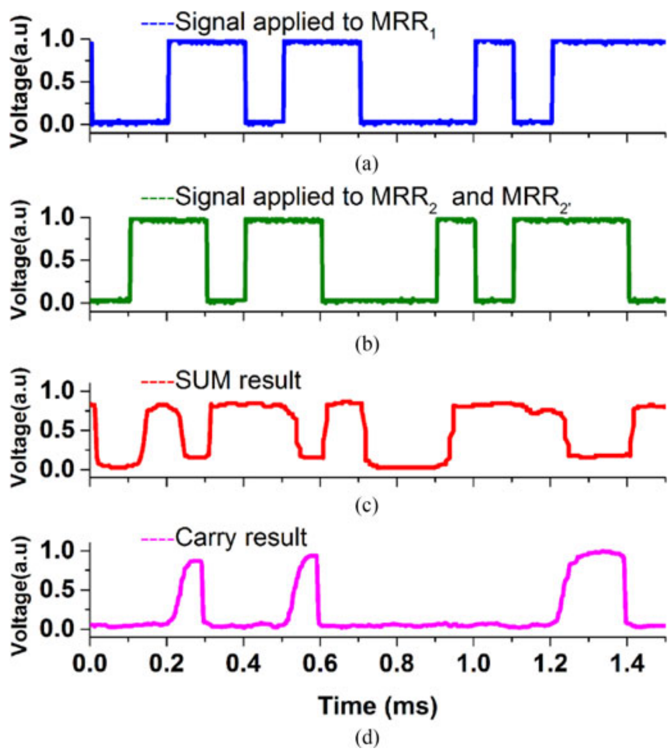

Fig. 6. Signals applied to (a) MRR_1, (b) MRR_2, and MRR_2, (c) the SUM result at the S port, and (d) the Carry result at the C port.

the two output ports of the device are fed into a high-speed photo-detector. And the electrical signals output from the detector are fed into an oscilloscope for waveform observation. Binary sequences Non-Return to Zero(NRZ) signals with the speed of 10 Kbps generated by the AFGs are applied to the Micro-heaters embedded around MRRs (The high-level is 2.05 V, and the low-level is 0 V). MRR_1's working states is controlled by the working states of the electrical signal X. On the other hand, MRR_2 and $MRR_{2'}$ are working as a synchronous part, and the working states are controlled by the electrical signal Y. It is shown in Fig. 6 that the circuit can performs the half-add operation correctly by the speed of 10 kbps. In our experimental tests, the laser input power is about 15.4 mw. Besides, the coupling loss to the silicon photonics device is about 2.7 dB at each end face. And the power consumption is about 5mW for each MRR when the voltages applied to them are at the high level. It is easy to draw that the rise time (10%–90%), and the fall time (90%–10%) is about 44 μs and 2 μs, respectively. In the design and testing process need to pay more attention to the following points:

1) In chip design, the rings should be as close as possible to prevent the limitation of fabrication accuracy of the deviation, and thermal crosstalk would exist when the rings are close enough. An ideal solution is fabricate some air trenches between the rings to block the spread of heat.
2) The limitation of fabrication accuracy of the deviation should be controlled to be as small as possible during the experimental test. A redshift can be measured when the MRR is heated up by the tunable voltage source, which derives from the effective refractive index of the ring increases. Therefore, the rings with shorter resonant wavelengths at the working wavelength needs to be compensated.

Compared with [44], the structure becomes relatively simpler (the MMI is eliminated in the device, and there is no multi-coupling region in the device). What's more, the experimental results are much better than those demonstrated devices. In the dynamic response of previous demonstration, logical 1 is represented by two stages of optical power at the output port sum, and in this paper, logical 1 is represented by only one stage. In addition, output signal quality is improved significantly. As we known, other advanced modulation schemes such as electro-optic modulation scheme can also be employed to modulate MRR, which can achieve a higher modulation speed. In future, advanced modulation such as reversely biased PN junction through the plasma dispersion effect and highly accurate manufacturing technology can be exploited to improve the operation speed of the device [17], [50].

5. Conclusion

In conclusion, we have reported a novel schematic which can perform the half-add operations based on cascaded MRRs. Compared to the previous structure, MMI and multi-coupling regions in a single MRR are eliminated in the proposed circuit, which are beneficial to reduce the insertion loss and crosstalk of the device. For proof of principle, a half-adder based on thermo-optic effect is fabricated. The device is demonstrated successfully at the speed of 10 kbps, and the signal quality is improved significantly.

References

[1] M. Hochberg and T. Baehr-Jones, "Towards fabless silicon photonics," *Nature Photon.*, vol. 4, pp. 492–494, 2010.
[2] D. Miller, "Device requirements for optical interconnects to CMOS silicon chips," in *Proc. Integr. Phonton. Res., Silicon Nanophoton. Photon. Switching*, 2010, Paper PMB3.
[3] M. A. Foster *et al.*, "Broad-band optical parametric gain on a silicon photonic chip," *Nature*, vol. 441, pp. 960–963, 2006.
[4] L. Yang *et al.*, "Reconfigurable nonblocking 4-port silicon thermo-optic optical router based on Mach–Zehnder optical switches," *Opt. Lett.*, vol. 40, pp. 1402–1405, 2015.
[5] A. Fu and P. Yang, "Organic-inorganic perovskites: Lower threshold for nanowire lasers," *Nature Mater.*, vol. 14, pp. 557–558, 2015.
[6] X. Zheng *et al.*, "A high-speed, tunable silicon photonic ring modulator integrated with ultra-efficient active wavelength control," *Opt. Exp.*, vol. 22, pp. 12628–12633, 2014.
[7] K. Bédard *et al.*, "Dual phase-shift bragg grating silicon photonic modulator operating up to 60 Gb/s," *Opt. Exp.*, vol. 24, pp. 2413–2419, 2016.
[8] C. Sturm *et al.*, "All-optical phase modulation in a cavity-polariton Mach–Zehnder interferometer," *Nature Commun.*, vol. 5, 2014, Art. no. 3278.
[9] C. Qiu, W. Gao, R. Soref, J. T. Robinson, and Q. Xu, "Reconfigurable electro-optical directed-logic circuit using carrier-depletion micro-ring resonators," *Opt. Lett.*, vol. 39, pp. 6767–6770, 2014.
[10] S. Lin, Y. Ishikawa, and K. Wada, "Demonstration of optical computing logics based on binary decision diagram," *Opt. Exp.*, vol. 20, pp. 1378–1384. 2012.
[11] H. Wei, Z. Wang, X. Tian, M. Käll, and H. Xu, "Cascaded logic gates in nanophotonic plasmon networks," *Nature Commun.*, vol. 2, 2011, Art. no. 387.
[12] F. T. Dullo *et al.*, "Sensitive on-chip methane detection with a cryptophane-A cladded Mach-Zehnder interferometer," *Opt. Exp.*, vol. 23, pp. 31564–31573, 2015.
[13] A. Psarouli *et al.*, "Monolithically integrated broad-band Mach-Zehnder interferometers for highly sensitive label-free detection of biomolecules through dual polarization optics," *Sci. Rep.*, vol. 5, 2015, Art. no. 17600.
[14] M. Ye, Y. Yu, G. Chen, Y. Luo, and X. Zhang, "On-chip WDM mode-division multiplexing interconnection with optional demodulation function," *Opt. Exp.*, vol. 23, 2015, Art. no. 32130.
[15] C. Sun *et al.*, "Single-chip microprocessor that communicates directly using light," *Nature*, vol. 528, pp. 534–538, 2015.

[16] C. Koos *et al.*, "All-optical high-speed signal processing with silicon–organic hybrid slot waveguides," *Nature Photon.*, vol. 3, pp. 216–219, 2009.
[17] A. Liu *et al.*, "High-speed optical modulation based on carrier depletion in a silicon waveguide," *Opt. Exp.*, vol. 15, pp. 660–668, 2007.
[18] D. Dai, J. Wang, and Y. Shi, "Silicon mode (de) multiplexer enabling high capacity photonic networks-on-chip with a single-wavelength-carrier light," *Opt. Lett.*, vol. 38, pp. 1422–1424, 2013.
[19] A. Liu *et al.*, "Wavelength division multiplexing based photonic integrated circuits on silicon-on-insulator platform," *IEEE J. Sel. Topics Quantum Electron.*, vol. 16, no. 1, pp. 23–32, Jan./Feb. 2010.
[20] L. Liu *et al.*, "An ultra-small, low-power, all-optical flip-flop memory on a silicon chip," *Nature Photon.*, vol. 4, pp. 182–187, 2010.
[21] R. Espinola, M. Tsai, J. T. Yardley, and R. Osgood, "Fast and low-power thermooptic switch on thin silicon-on-insulator," *IEEE Photon. Technol. Lett.*, vol. 15, no. 10, pp. 1366–1368, Oct. 2003.
[22] Q. Xu, P. Dong, and M. Lipson, "Breaking the delay-bandwidth limit in a photonic structure," *Nature Phys.*, vol. 3, pp. 406–410, 2007.
[23] M. H. Khan *et al.*, "Ultrabroad-bandwidth arbitrary radiofrequency waveform generation with a silicon photonic chip-based spectral shaper," *Nature Photon.*, vol. 4, pp. 117–122, 2010.
[24] S.-H. Chang, "A dishing model for chemical mechanical polishing of metal interconnect structures," *Microelectron. Eng.*, vol. 77, pp. 76–84, 2005.
[25] G. Hajisalem, M. S. Nezami, and R. Gordon, "Probing the quantum tunneling limit of plasmonic enhancement by third harmonic generation," *Nano Lett.*, vol. 14, pp. 6651–6654, 2014.
[26] B. Little, S. Chu, W. Pan, and Y. Kokubun, "Microring resonator arrays for VLSI photonics," *IEEE Photon. Technol. Lett.*, vol. 12, no. 3, pp. 323–325, 2000.
[27] J. Hryniewicz, P. Absil, B. Little, R. Wilson, and P. Ho, "Higher order filter response in coupled microring resonators," *IEEE Photon. Technol. Lett.*, vol. 12, no. 3, pp. 320–322, Mar. 2000.
[28] Y. Ding *et al.*, "Effective electro-optical modulation with high extinction ratio by a graphene–silicon microring resonator," *Nano Lett.*, vol. 15, pp. 4393–4400, 2015.
[29] Q. Li *et al.*, "A 10-Gb/s silicon microring resonator-based BPSK link," *IEEE Photon. Technol. Lett.*, vol. 26, no. 18, pp. 1805–1808, Sep. 2014.
[30] I. Amiri and J. Ali, "Single and multi optical soliton light trapping and switching using microring resonator," *Quantum Matter*, vol. 2, pp. 116–121, 2013.
[31] A. L. Giesecke *et al.*, "Add-drop microring resonator for electro-optical switching and optical power monitoring," in *Proc. Conf. Lasers Electro-Opt., Sci. Innov.*, 2014, Paper STh4M. 2.
[32] H. Yan, X. Feng, D. Zhang, and Y. Huang, "Integrated optical add-drop multiplexer based on a compact parent-sub microring-resonator structure," *Opt. Commun.*, vol. 289, pp. 53–59, 2013.
[33] A. C. Turner, M. A. Foster, A. L. Gaeta, and M. Lipson, "Ultra-low power parametric frequency conversion in a silicon microring resonator," *Opt. Exp.*, vol. 16, pp. 4881–4887, 2008.
[34] X. Yan, C.-S. Ma, C.-T. Zheng, X.-Y. Wang, and D.-M. Zhang, "Analysis of polymer electro-optic microring resonator switches," *Opt. Laser Technol.*, vol. 42, pp. 526–530, 2010.
[35] B. Guha, B. B. Kyotoku, and M. Lipson, "CMOS-compatible athermal silicon microring resonators," *Opt. Exp.*, vol. 18, pp. 3487–3493, 2010.
[36] Q. Xu and R. Soref, "Reconfigurable optical directed-logic circuits using microresonator-based optical switches," *Opt. Exp.*, vol. 19, pp. 5244–5259, 2011.
[37] J. Hardy and J. Shamir, "Optics inspired logic architecture," *Opt. Exp.*, vol. 15, pp. 150–165, 2007.
[38] C. Qiu, X. Ye, R. Soref, L. Yang, and Q. Xu, "Demonstration of reconfigurable electro-optical logic with silicon photonic integrated circuits," *Opt. Lett.*, vol. 37, pp. 3942–3944, 2012.
[39] Z. Pei-Ji *et al.*, "Strictly non-blocking 4 $\times$ 4 silicon electro–optic switch matrix," *Chin. Phys. B*, vol. 24, 2015, Art. no. 124209.
[40] L. Zhang *et al.*, "Demonstration of directed XOR/XNOR logic gates using two cascaded microring resonators," *Opt. Lett.*, vol. 35, pp. 1620–1622, 2010.
[41] L. Lu *et al.*, "4 $\times$ 4 silicon optical switches based on double-ring-assisted Mach–Zehnder interferometers," *IEEE Photon. Technol. Lett.*, vol. 27, no. 23, pp. 2457–2460, Dec. 2015.
[42] B.-C. Han *et al.*, "Experimental study on all-optical half-adder based on semiconductor optical amplifier," *Optoelectron. Lett.*, vol. 5, pp. 161–164, 2009.
[43] R. Cuykendall and D. R. Andersen, "Reversible optical computing circuits," *Opt. Lett.*, vol. 12, pp. 542–544, 1987.
[44] Y. Tian *et al.*, "Directed optical half-adder based on two cascaded microring resonators," *IEEE Photon. Technol. Lett.*, vol. 24, no. 8, pp. 643–645, Apr. 2012.
[45] Y. Huang, X. Duan, Y. Cui, L. J. Lauhon, K.-H. Kim, and C. M. Lieber, "Logic gates and computation from assembled nanowire building blocks," *Science*, vol. 294, pp. 1313–1317, 2001.
[46] T. Tsuchizawa *et al.*, "Fabrication and evaluation of submicron-square Si wire waveguides with spot size converters," in *Proc. 15th Annu. Meeting IEEE Lasers Electro-Opti. Soc.*, 2002, pp. 287–288.
[47] N. Sherwood-Droz *et al.*, "Optical 4 $\times$ 4 hitless silicon router for optical networks-on-chip (NoC)," *Opt. Exp.*, vol. 16, pp. 15915–15922, 2008.
[48] J. Scheuer, "Fabrication and characterization of low-loss polymeric waveguides and micro-resonators," in *Proc. Integr. Photon. Nanophoton. Res. Appl.*, 2007, Paper ITuA3.
[49] H. Hodaei *et al.*, "Parity-time–symmetric microring lasers," *Science*, vol. 346, pp. 975–978, 2014.
[50] L. Yang, L. Zhang, C. Guo, and J. Ding, "XOR and XNOR operations at 12.5 Gb/s using cascaded carrier-depletion microring resonators," *Opt. Exp.*, vol. 22, pp. 2996–3012, 2014.